

The effect of surfactant monolayers on vortex rings formed from an impacting water drop

J. R. Saylor^{a)} and N. K. Grizzard

Clemson University, Department of Mechanical Engineering, Clemson, South Carolina 29634

(Received 3 January 2003; accepted 1 July 2003; published 26 August 2003)

The impact of a falling drop with a flat liquid surface can result in the formation of a subsurface vortex ring that penetrates a significant distance into the liquid bulk. Herein an experimental study of these vortex rings is presented for water drops striking a water surface. The effect of surfactant monolayers was investigated by measuring the vortex velocity for water surfaces that were free of surfactants, as well as surfaces covered with surfactant monolayers. A soluble and an insoluble monolayer were investigated, Triton X-100 and oleyl alcohol, respectively. Oleyl alcohol was investigated for concentrations ranging from 0 to $0.495 \mu\text{g}/\text{cm}^2$, and Triton X-100 was investigated for concentrations ranging from 0 to 4.0 mg/L. For both surfactants the vortex velocity displayed a maximum at intermediate surfactant concentrations. In all cases the drop fluid was free of surfactants. A possible mechanism based on capillary wave damping is presented to explain these results. The relevance of this work to rain over lakes and oceans is discussed. © 2003 American Institute of Physics. [DOI: 10.1063/1.1603225]

I. INTRODUCTION

When water drops impact a flat water surface from a low elevation, a vortex ring is formed beneath the water surface. These drop-induced vortex rings have been the focus of experimental and analytical investigation for over a century as will be described below. In spite of this long history of research, much about the processes which control the formation of these vortex rings is not well understood. However, it is generally agreed that surface tension plays an important role. Surfactants reduce the surface tension of an interface, and are frequently present on water surfaces. Yet the role of surfactants on drop-induced vortex formation has never been explored. Herein surfactant monolayers are applied to the flat water surface to determine their effect on drop-induced vortices. A review of the current understanding of drop-induced vortices is presented first.

Perhaps the first description of vortices formed by falling drops is that due to Rogers¹ who in 1858 described drop-induced vortices as one of several methods for forming vortex rings. He noted that good rings could be obtained by releasing a drop from a height beneath about one and one-half inches. The first detailed study of drop-induced vortices appears to be that due to Thomson and Newall² who in 1885 investigated a plethora of fluids in an attempt to understand the phenomena. Several important results were uncovered during their work. One of particular importance was the observation that the penetration depth of the vortex depended on the height from which the drop was released. The penetration depth is defined as the distance beneath the surface that the vortex travels before it stops moving. Thomson and Newall² showed that the vortices penetrated particularly well

for certain heights, and quite poorly for others. A plot of vortex penetration depth versus drop release height was oscillatory in nature. The authors related the spacing between the peaks in these plots to a temporal spacing using the velocity and acceleration of the falling drop. They found that the time intervals between the peaks agreed very well with the oscillation period of a drop about its equilibrium shape. Hence, it was implied that some aspect of the oscillation of the falling drop accounted for the variations in vortex penetration depth.³

Chapman and Critchlow⁴ confirmed and extended the results of Thomson and Newall² using photographs to record the shape of the drop as it fell. As alluded to above, a falling drop oscillates as it falls, attaining ellipsoidal shapes that vary from an oblate form at one extreme to a prolate form at the other, and attaining a spherical shape in between. In this paper oblate refers to an ellipsoid with its major axis in the horizontal orientation, and prolate refers to an ellipsoid with its major axis in the vertical orientation. The photographs of Chapman and Critchlow⁴ revealed that the vortices that penetrated the farthest were obtained from drops having specific shapes at impact. The vortex penetration depth was observed to achieve a maximum when the drop was spherical at impact, and in the process of transitioning from an oblate spheroid to a prolate spheroid. Conversely, when the drop was spherical and moving from a prolate to an oblate shape, vortex penetration was at a minimum. The authors suggested that the reason for these observations was related to the internal velocity field of the oscillating drop.⁵⁻⁷

A study very similar to that of Chapman and Critchlow⁴ was conducted by Durst⁸ who obtained the same conclusions regarding the drop shape at which vortex penetration was maximized. However, a comparable study by Rodriguez and Mesler⁹ who recorded the shape of the drop at impact using high speed motion pictures (some of which are reproduced in

^{a)} Author to whom correspondence should be addressed. Electronic mail: jrsaylor@ces.clemson.edu

their paper) found that the most penetrating vortices were observed when the drop was prolate in shape and minimum penetration occurred when the drop was oblate. An explanation for these observations was related to the shape of the crater and how different crater shapes were formed as a result of drops of differing shape. A study due to Peck and Sigurdson¹⁰ also suggests the importance of the impact crater.

The aforementioned studies differ with regard to the proper drop shape needed for maximal vortex penetration, however, they all share a topological approach to investigating drop-induced vortices. Moreover, these studies focus on the peak *locations* in the vortex penetration versus drop height plots. Studies focusing on factors which may affect the *amplitudes* of these peaks have not been conducted. In the present work we focus on the amplitudes of these peaks and seek to ascertain the role that surfactants play in modulating these peaks.

Surfactants affect the surface elasticity, the surface viscosity and the surface tension. They have never been explored explicitly with regard to drop-induced vortices, however, some research on the role of surface tension in drop-induced vortices already exists. For example, the role of surface tension was investigated indirectly by Thomson and Newall² who used many different liquids in their study, covering a large range in surface tension. However, they only reported qualitative characterizations of the vortices; no results regarding the penetration depth were provided. Chapman and Critchlow⁴ provide data on 16 different liquids, including water, giving a range in surface tension from $\sigma = 0.08\text{--}72.8$ dynes/cm. In this work they correlated the location of the first peak in their drop height versus penetration depth plot to the parameter $\sigma/\rho g$, where σ is surface tension, ρ is liquid density, and g is the gravitational acceleration. However, no attempt was made to correlate the penetration depth to this or any other parameter.

In the present study the surface tension of the flat water surface is varied by applying surfactant monolayers in varying concentrations. In this way the surface tension is altered without significantly changing any bulk fluid property. The surface tension of the drop liquid is left unchanged. Hence, any change in the surface tension of the flat water surface manifests itself as a change in the *difference* in surface tension between the drop and bulk liquid. This is significant since an application of the present work is rain enhanced gas exchange by drop-induced vortices, where the surface tension of the drop and flat surface are usually different. This is discussed further below. Using surfactants to change the surface tension of the drop is also possible, however there are added complications with this approach. While there are methods for conducting this type of experiment, they are not explored here.

An application of the present work pertains to the enhancement of air–water gas exchange by rain. Rain is known to enhance transport between surface fluid and subsurface water, thereby enhancing gas exchange.^{11,12} The formation of vortices, along with several other phenomena, is believed to be responsible for this enhanced gas exchange.

The primary impact of a raindrop does not typically

form a vortex. The splash caused by an impacting raindrop results in a vertically rising jet which typically forms a secondary drop. This secondary drop can form a vortex when it returns to the water surface. Lange *et al.*¹³ studied the turbulence formed by simulated raindrops and observed the formation of vortices from these secondary drops using both dye imaging and particle image velocimetry. A splash can also result in a coronet or crown which is a circular film of fluid emanating outward from the crater which can become unstable and break down into many small drops. Although the formation of vortices from these crown drops has not been documented, it seems that they should also be very effective in this regard since they impact the water surface from a small height.

The significance of the raindrop formed vortices concerns the mixing which they impart. The transport of dissolved gases such as oxygen and carbon dioxide from the air into a lake or ocean is limited by the diffusion-controlled concentration boundary layers which exist on the water side of the free surface. Any mechanism which enhances the transfer of fluid from these boundary layers into the bulk can substantially increase transport since larger scale currents are effective in transporting fluid deep into the bulk, once the fluid is away from the free surface. The enhancement of gas exchange by drop-induced vortices is significant with regard to carbon dioxide sequestration, a key process in understanding global climate processes. This mixing process is also important with regard to oxygenation of lakes. Durst⁸ observed that oxygen concentration profiles in lakes exhibited a maximum beneath the surface, a result that can be explained by vortex penetration and cannot be explained by turbulent or gradient driven transport alone.

In both oceanic and limnological applications the surface tension of the raindrop and of the ocean or lake surface are dissimilar. In oceanic applications, the surface tension of sea water is larger than that of the raindrop due to the presence of salt. In lakes, surfactant monolayers caused by bioactivity are omnipresent and serve to reduce the surface tension with respect to the relatively cleaner raindrop surface. Hence in both cases the raindrop and the flat surface have different surface tensions. The present study addresses a situation very similar to the limnological application, since the drop is nominally free of surfactants and the flat water surface is covered with a surfactant monolayer. In oceanic applications, surfactants are frequently present as well, especially in near-shore regions.

The work presented here details the drop-induced vortices formed by single drops striking an undisturbed surface. Of course in an actual rain event, many drops would be striking the water surface simultaneously and there would be numerous interactions between rain drops and splash drops. The work presented here does not address this more complicated situation since the behavior of single drops is still poorly understood.

II. EXPERIMENTAL METHOD

In the research cited above the characteristics of drop-induced vortices were quantified by a penetration depth. This

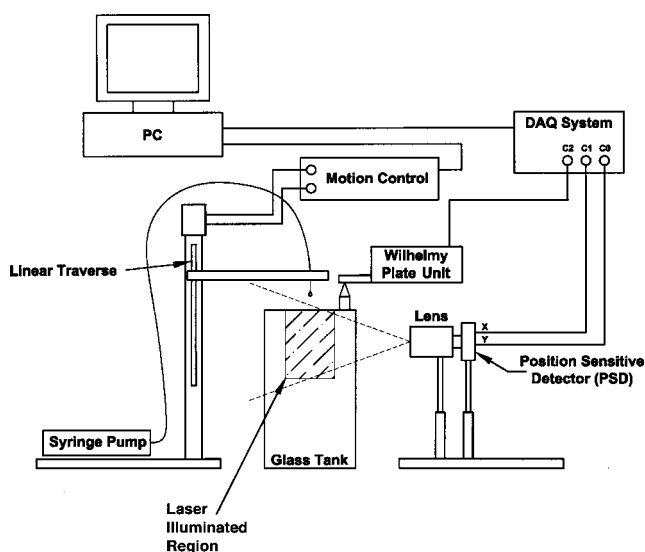


FIG. 1. Experimental apparatus. Note that the laser beam is directed out of the plane of the page in this figure.

approach was attempted during preliminary experiments in the present study. However, the necessarily subjective nature of deciding when a vortex had stopped moving was found to be unsatisfactory. At some point in the deceleration of the vortex, small natural convection currents began to dominate and deciding when the vortex had truly stopped moving was difficult. Accordingly we chose to characterize the vortex by its velocity. Vortex velocity was measured at a fixed location beneath the surface. A strong correlation between vortex velocity and vortex penetration is expected from visual observations in our tank. Results presented in Chapman and Critchlow⁴ show that vortices decelerate at a constant rate, further supporting this correlation.

A. Apparatus

The apparatus used in these experiments is shown schematically in Fig. 1. This apparatus generated the drops and resulting vortex rings and recorded the vortex velocities, surface tension and other relevant variables.

Drops used to create vortices were formed at the end of a 1.6 mm outside diameter Teflon tube. This tube was connected to a syringe pump which supplied a slow flow of dyed liquid. The pump flow rate could be controlled to ± 0.1 mL/hr. The tip of the Teflon tube was mounted on a support arm which was connected to a stepper-motor-driven vertical traverse. The stepper motor was controlled by a motion controller card installed in the PC, allowing for exact positioning of the tube tip, and hence the drop release height. This motion control system operated with a precision of ± 0.02 mm. The drops formed by the syringe pump system were found to vary in volume by less than ± 0.3 μ L. The average drop volume was 24.8 μ L, giving an effective drop diameter of 3.6 mm. The drop fluid was doubly distilled water containing fluorescein dye. The fluorescein dye concentration was smaller than 0.25 mg/L in all cases. Experiments were conducted in standard room conditions where

temperature ranged from 18 to 22 °C, and relative humidity ranged from 15%–60%.

Three signals were recorded during the experiments. Two of these were the x and y components of a position sensitive detector (PSD) that was used to measure the vortex velocity as is described later in this section. The third signal was the output of the surface tensiometer which recorded surface tension using a Wilhelmy plate. All three signals were recorded by the PC using a data acquisition card. Data acquisition and motion control were automated using a program written in the LABVIEW environment. The entire experimental apparatus was located in a 0.5 \times 2.0 meter laminar flow hood to provide a clean, controlled environment for the experiments. The laminar flow hood caused significant vibration during fan operation, so the fan was only run between experiments. Opaque Plexiglas and cardboard sheets were used to shield the work area from potentially disturbing air currents and light interference from the room. A 0.6 \times 1.3 meter optical breadboard was placed in the laminar flow hood and used to fasten securely the equipment and optics.

The water tank in which vortex rings were created was made of 0.6 cm thick flat glass panels. These were cut and ground on the edges, and RTV (type 110) silicon adhesive was used to bond the panels together. The vortex tank interior width, depth, and height dimensions measured 16.0 cm \times 16.0 cm \times 40.0 cm, respectively. The walls of the tank were separated by a distance large enough to eliminate any interference between the vortex and the walls. This actually could have been achieved with a much smaller tank; the larger tank used here was chosen to reduce the buildup of fluorescein dye from the drops, allowing longer periods of operation without emptying and refilling the tank.

Two 1.0 cm diameter holes located 5.0 cm from the tank bottom were used for filling and emptying the tank. Teflon tubing was connected to these holes and fastened into place with RTV silicon adhesive. One tubing line was routed to a fill reservoir, and the second to a drain. Teflon valves were used to control the flow in and out of the vortex tank. The tank was designed to operate with the water level at the tank rim. This facilitated the swipe and overflow surface cleaning procedures, which are described in Sec. II B. The tank itself was placed in a Plexiglas overflow basin, which was a shallow plastic box with a hole for draining. Periodically during these experiments the entire tank was emptied and swabbed with Kimberly–Clark low lint Kimwipes (type EX-L) soaked with high performance liquid chromatography (HPLC) grade methanol. It was then rinsed with HPLC grade methanol and then with doubly distilled water. Powderless latex gloves were worn during all cleaning procedures.

Water was supplied to the tank via a 50 L low density polyethylene (LDPE) carboy located approximately one meter above the tank surface. The carboy was frequently cleaned with HPLC grade methanol and immediately rinsed with doubly distilled water. After cleaning, it was filled only with doubly distilled water. The vortex tank was filled from a valve at the bottom of the carboy. Any surfactant contamination in the carboy is expected to rise to the water surface in the carboy. Therefore, surfactant contamination is prevented

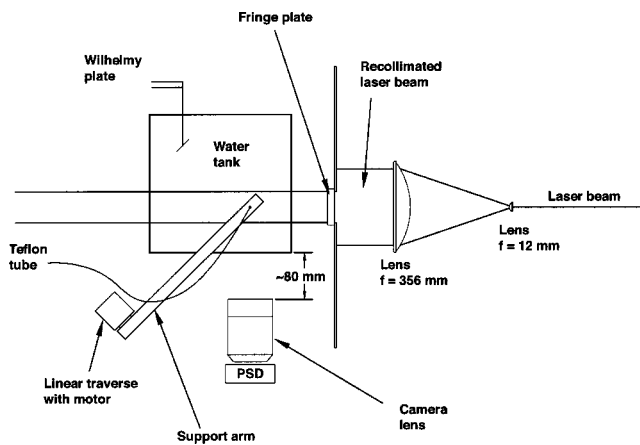


FIG. 2. Top view of apparatus.

from entering the vortex tank by filling the tank from the carboy bottom.

Surface tension was measured with a Sigma 703 tensiometer (KSV Instruments Ltd.) with a platinum Wilhelmy plate attachment. The location of the Wilhelmy plate with respect to the drop location and the tank edges is indicated in Fig. 2. The lower edge of the Wilhelmy plate was attached to the water surface. The force exerted on the plate was used to measure the surface tension via the relation

$$\frac{W_{\text{tot}}}{p} = \frac{W_{\text{plate}}}{p} + \sigma, \quad (1)$$

where p is the perimeter of the Wilhelmy plate edge in contact with the water surface, W_{tot} is the total force measured by the tensiometer and W_{plate} is the weight of the plate. This relation assumes a zero contact angle between the liquid meniscus and the Wilhelmy plate. The surface tension of clean water at 25 °C is 71.97 dynes/cm.¹⁴ Using the Wilhelmy plate to measure the surface tension of doubly distilled water, a value of 72.0 dynes/cm was obtained and remained stable for several hours when exposed to laboratory air. The surface tension of the stock solution of fluorescein dye that was used to create the drop fluid had a concentration of 10 mg/L, and had a measured surface tension of 72.0 dynes/cm. Therefore, the surface tension of the dyed drops which contained the stock fluorescein solution diluted by doubly distilled water was assumed to be 72.0 dynes/cm during the experiments.

The Wilhelmy plate was cleaned frequently by rinsing the plate thoroughly with HPLC grade methanol and then with distilled water. The plate was also periodically heated with a propane torch until it glowed red to eliminate any organic contaminants from the plate. After this process it was allowed to cool, and was then rinsed with HPLC grade methanol and water to remove any combustion residue. These cleaning procedures were recommended by the manufacturer.

Laser induced fluorescence (LIF) was used to visualize the vortices. The drop fluid consisted of a solution of fluorescein and water. When a drop fell to the water surface, a vortex ring was formed and the dye in the drop fluid was incorporated into the vortex. The subsurface region was illuminated by a 750 mW argon ion laser. Fluorescence from the

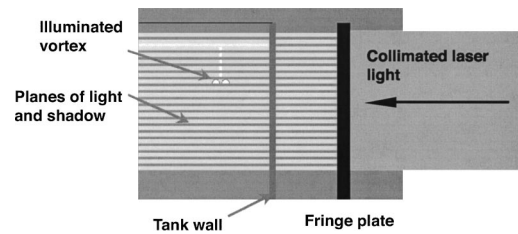


FIG. 3. Schematic of the measurement region. The fringe plate blocks part of the collimated laser beam, creating horizontal planes of light and shadow.

dye was collected and focused onto a photodetector to record velocity as is described below. To create a larger volume of illumination (reducing the chance that the vortex would not be seen), the laser was expanded. The beam was directed through a 12 and 356 mm focal length lens combination, separated by the sum of their focal lengths as illustrated in Fig. 2. This expanded the beam to approximately 15 cm in diameter. Due to the Gaussian distribution of the laser beam, only the inner ~8 cm of the column was bright enough to illuminate the vortex to a significant extent. This 8 cm inner beam was directed through the tank where velocity measurements were made.

The photodetector used to measure vortex velocity was a position sensitive detector (PSD). The x and y outputs of a PSD are linearly related to the x and y location of the centroid of light striking the detector. Hence, as the vortex travels across the region imaged onto the PSD, the illumination centroid moves and the x and y outputs of the PSD are modulated accordingly. A 55 mm focal length camera lens was used to focus the measurement region onto the PSD. The lens and PSD were positioned closely to the tank so that the field of view would only include the brightly illuminated portion of the bulk fluid. The outputs of the PSD were connected to the PC data acquisition card, and data were acquired at 1000 Hz.

Although the vortex appeared to fluoresce brightly when illuminated by the laser, its motion did not modulate the PSD outputs to a sufficient extent. To increase the sensitivity of the PSD signal to vortex motion, a fringe plate was placed in front of the laser beam to create alternating illuminated and shadowed planes in the tank. As the vortex travels through these slabs of light, it alternately fluoresces brightly and then becomes invisible. By moving the PSD slightly off the optical axis of the camera lens, a particularly well-modulated PSD signal resulted. The laser fringes were equally separated in space. The time separation of the peaks in the PSD time trace corresponded to the time it took the vortex to travel one fringe spacing. These time separations in the PSD signal and the linear separation of the fringes in the tank were used to obtain the vortex velocity v using the equation

$$v = \frac{\Delta x}{\Delta t}, \quad (2)$$

where Δx is half the fringe spacing and Δt is half the pulse spacing obtained from the PSD signal (the reason for using half spacing is described below).

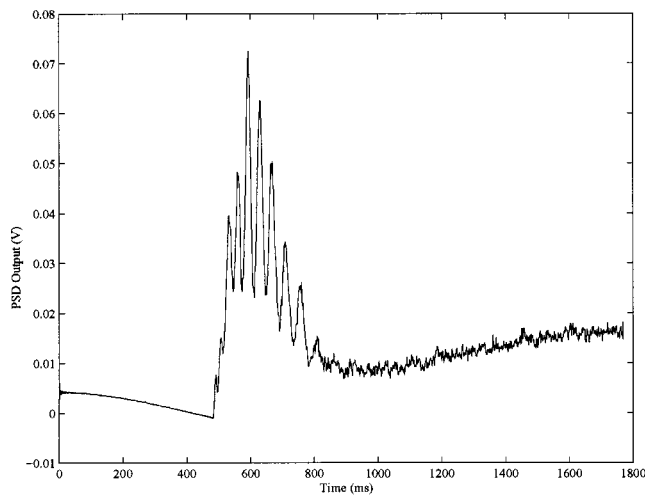


FIG. 4. Plot of PSD output voltage versus time, sampled at 1000 Hz. Motion of the vortex through the laser beam fringes causes the peaks and dwells in the signal.

The fringe plate was made from 1.59 mm diameter rods which fit in a frame having a series of V-groves separated by 1/8 of an inch. Hence, the fringe spacing was 0.125 inches. A schematic of the equally spaced horizontal sheets of light created by the fringe plate is illustrated in Fig. 3. A typical PSD signal obtained from a vortex traveling through the fringed laser beam is shown in Fig. 4. The pulses become larger in intensity as the vortex travels through the measurement volume due to the Gaussian nature of the laser beam. The fringes near the beam center are brighter than those at the edge, resulting in a greater displacement of the light centroid on the PSD.

Vortex velocities were obtained from the PSD time traces, such as the one presented in Fig. 4, using a computer program written in MATLAB. This code located the highest peak in the time trace and then located peaks and dwells to the right of this largest peak (peaks to the left of the main peak were fewer, and not as easily recognizable for weak signals). The time separation between (i) the main peak and the first dwell, (ii) the first dwell and second peak, and (iii) the second peak and second dwell were then identified by this code. From these three time differences, velocities were computed using the Δt between each peak and dwell according to Eq. (2). Because this time spacing corresponds to the vortex traveling from a bright region to a dark region (and not between two bright regions), Δx in Eq. (2) is half the fringe spacing, or 0.0625 inches. The three velocities obtained in this way were compared; if they did not deviate by a large amount (indicative of noise or some other problem with the time trace), they were averaged and recorded as an acceptable vortex velocity. If the deviation was too large, the signal was discarded. If the vortex velocity fell beneath a minimum threshold, it too was discarded. This minimum velocity was the measured fall speed of a dye parcel laid upon the water surface.

The physical location corresponding to the highest peak in the time trace was determined by placing an object in the tank so that it scattered light into the PSD. This object was

progressively lowered while observing the PSD output. The point at which a maximum in the PSD output was observed was recorded. This depth was 14 mm. Hence, the peak in the PSD signals like that in Fig. 4 always occurred at a location 14 mm beneath the surface. Therefore, the velocity obtained from the algorithm described above corresponds to a velocity measurement of the vortex at a location 14 mm beneath the water surface.

Experiments with drop-induced vortex rings require special care because ring formation is known to be highly sensitive to environmental conditions.^{10,15,16} To reduce scatter in the data, the entire experimental apparatus was placed in a laboratory hood (with the fan turned off) so that it was enclosed on all sides but one, reducing the effect of any room air currents. The tank was also supported by four rubber feet to isolate it from building vibrations. In spite of these precautions, the scatter in the data was not insignificant. Steps which could have further reduced the scatter such as the use of a vibration isolation table and a customized temperature control system were not implemented since they were not available.

B. Experimental procedure

Surfactant monolayers were created on the water surface by depositing a prepared stock solution of the surfactant. Two surfactants were investigated, oleyl alcohol and Triton X-100. The oleyl alcohol stock solution concentration was 0.85 mg/mL, and the Triton X-100 stock concentration was 4 mg/mL.

For experiments where an oleyl alcohol monolayer was to be applied to the water surface, the tank was filled to the rim with doubly distilled water from the elevated carboy reservoir, and then over filled for a short time to remove any contamination on the water surface. The surface was then swiped with a glass rod to remove any contamination that still remained. A 10 μ L glass syringe was used to apply a carefully controlled volume of the heptane and oleyl alcohol stock solution to the water surface. Care was taken to insure that all of this solution was placed on the surface and not injected into the bulk. The heptane-oleyl alcohol solution formed a liquid lens when deposited on the water, floated for several seconds and then evaporated leaving an oleyl alcohol monolayer.

When a Triton X-100 monolayer was required, the tank was first filled and the water surface was cleaned using the same procedure as described above for the oleyl alcohol monolayer preparation. The water level was then lowered by several centimeters and the Triton X-100 solution was added. Because surfactant can accumulate on the surface of bubbles and alter the surface concentration, the Triton X-100 solution was added slowly to prevent splashing and bubble formation. Using a clean glass rod, the solution was stirred gently but thoroughly. Once the added Triton X-100 was dissolved, the tank was filled and then overfilled very slightly. The surface was then swiped to remove any contaminating (non-Triton X-100) surfactant accumulated during mixing.

For experiments conducted without any surfactants (surfactant concentration of zero), doubly distilled water was

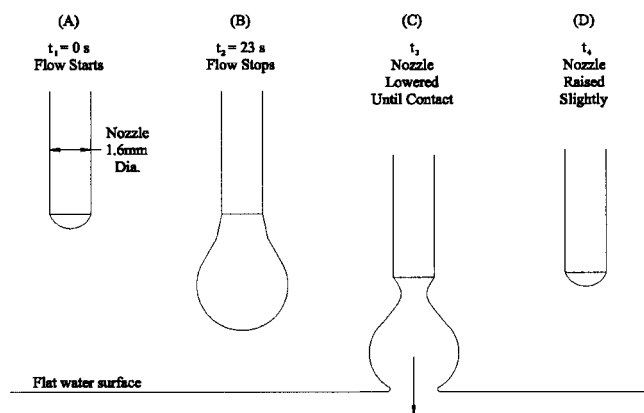


FIG. 5. Illustration of the procedure used to define the lowest drop height.

added to the tank. The tank was overflowed and swiped with a glass rod, and experiments were then initiated. When switching from one surfactant to another, or when switching from a surfactant run to a zero concentration run, special care was taken to empty the tank completely and clean it prior to the next set of experiments.

Special care was required regarding the position of the drop nozzle with respect to the free surface. At very small nozzle heights, drops will touch the surface before detaching from the nozzle. These “pull-away-drops” do not have the same volume as drops that completely separate from the nozzle before impact. For this reason we chose not to investigate these drops and established a procedure to achieve the lowest possible nozzle height without creating pull-away-drops. This procedure is shown graphically in Fig. 5. First, the time between drops (as controlled by the syringe pump) was measured with the nozzle far from the water surface. This duration was just under 25 s. Next, a single drop was formed, and the syringe pump was stopped at approximately one second prior to the expected time of drop release [see Figs. 5(a) and 5(b)]. With this elongated drop suspended, the nozzle was slowly lowered until the drop merged with the water surface [Fig. 5(c)]. The translation stage was advanced in increments of just over 0.3 mm during this last step, to determine accurately the position where the drop merged with the surface. After drop contact, the nozzle was raised by a single 0.3 mm increment. This position was the lowest nozzle position from which a drop could form and completely release from the nozzle prior to impacting the flat surface, and was the lowest nozzle position investigated here. This position was 4.8 mm. Because any change in the meniscus of the tank would change the nozzle-to-surface dis-

TABLE I. Surfactant conditions for each experiment. For all experiments the drop fluid was free of surfactants.

Experiment	Surfactant	Concentration
1	Oleyl alcohol	$c = 0.0, 0.055, 0.110, 0.165, \text{ and } 0.495 \mu\text{g}/\text{cm}^2$
2	Triton X-100	$c = 0.0, 0.125, 0.25, 0.5, 1.0, 2.0, \text{ and } 4.0 \text{ mg/L}$

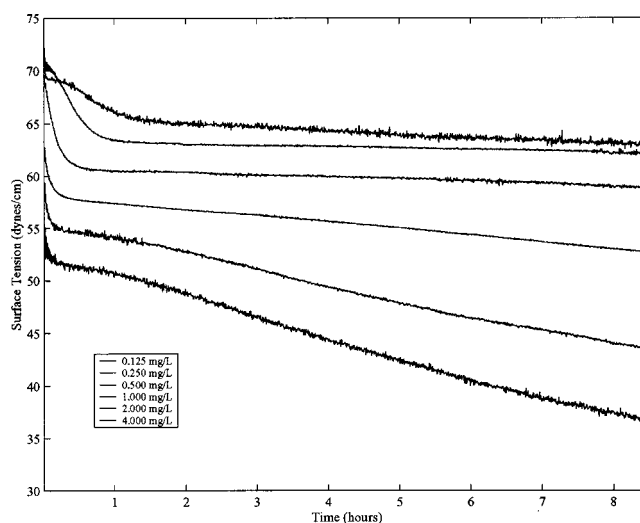


FIG. 6. Surface tension versus time for the Triton X-100 concentrations investigated. The Triton X-100 concentration increases from the highest plot to the lowest plot, as indicated in the legend.

tance, the above procedure was repeated each time the water level was disturbed due to swiping or overflow.

Two types of experiments were conducted: Oleyl alcohol monolayers were used in experiment #1, and Triton X-100 monolayers in experiment #2. Table I summarizes these experiments and the concentrations of each monolayer used.

For both sets of experiments the drop height range was 4.8–46.0 mm. Multiple vortices were recorded at each drop height. During the oleyl alcohol experiments, low concentration runs were conducted first. When the entire drop height range had been explored, the tank was overfilled for a short while and then swiped to remove the old monolayer. The higher concentration was then applied. By testing low concentrations first, the possibility of error introduced from oleyl alcohol buildup was significantly reduced. The inverse of this procedure was used for experiment #2 with Triton X-100, where the highest Triton X-100 concentration investigated was prepared first. The full drop height range was explored at this concentration, and the tank was then drained by 50% and filled again. This gave a new surfactant concentration of 2.0 mg/L. This procedure was continued until the concentrations $c = 4.0, 2.0, 1.0, 0.5, 0.25, \text{ and } 0.125 \text{ mg/L}$ were investigated. A zero concentration run was also conducted.

When forming an insoluble monolayer, the surfactant is placed directly on the surface. However, when forming a monolayer of a soluble surfactant, the monolayer is created by diffusion from the bulk liquid. Hence, after swiping, the surface concentration increases at an exponentially decaying rate. To ensure sufficient time for monolayer formation, the surface was left undisturbed for approximately 9 hours prior to each experimental session. Surface tension was monitored for the duration of this delay. A sample time trace of surface tension is presented in Fig. 6, beginning after swiping a Triton X-100 flat surface. As this figure illustrates, surface tension did not reach a fully stable condition even after more than 8 hours. Though surface tension was not completely

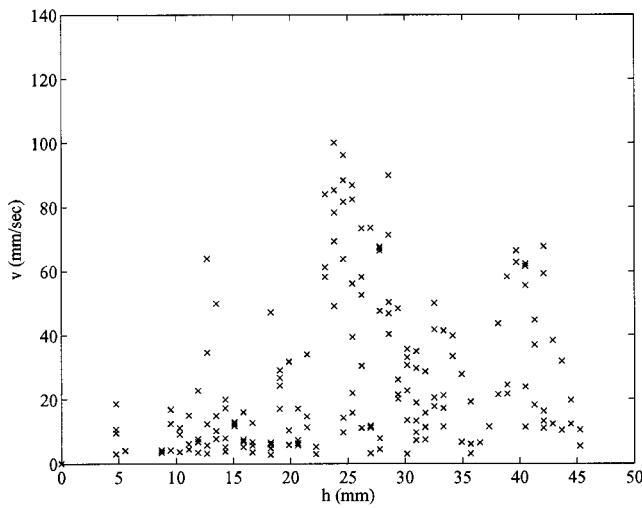


FIG. 7. Sample plot of v versus h . Each point corresponds to a single velocity measurement. This sample was for experiment #1 with an oleyl alcohol concentration of $c = 0.055 \mu\text{g}/\text{cm}^2$.

stable after such a long period of time, it was deemed necessary to conduct experiments after this period to avoid other problems such as contamination and evaporation. Accordingly, all experiments were conducted after a 9-hour time delay regardless of surface tension stability. To minimize changes from start to finish, experimental sessions were limited to 1.5 hours.

III. RESULTS

Plots of vortex velocity v versus drop height h are now presented. Drop height h is defined here to be the distance from the water surface to the nozzle.

A sample plot of vortex velocity v versus drop height h is presented in Fig. 7. This sample is from the experiment #1 case where the water surface was covered by a monolayer of oleyl alcohol at a concentration $c = 0.055 \mu\text{g}/\text{cm}^2$. A single data point is provided for each velocity measurement. All velocities in this plot and throughout this paper were re-

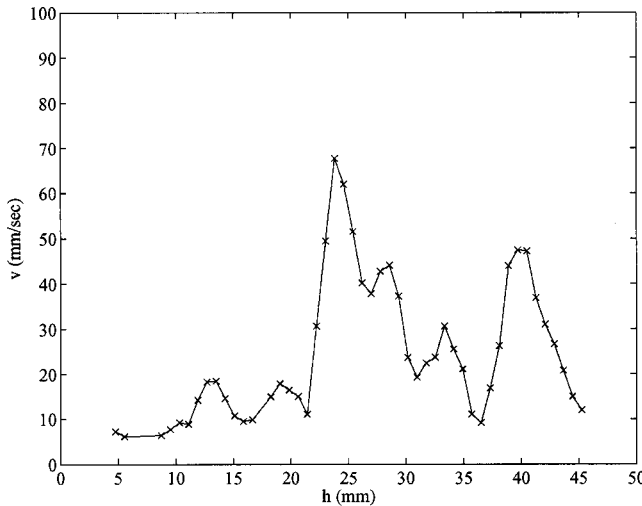


FIG. 8. Sample plot of averaged v versus h . Each point was found by averaging the points in Fig. 7 in bins consisting of three drop heights.

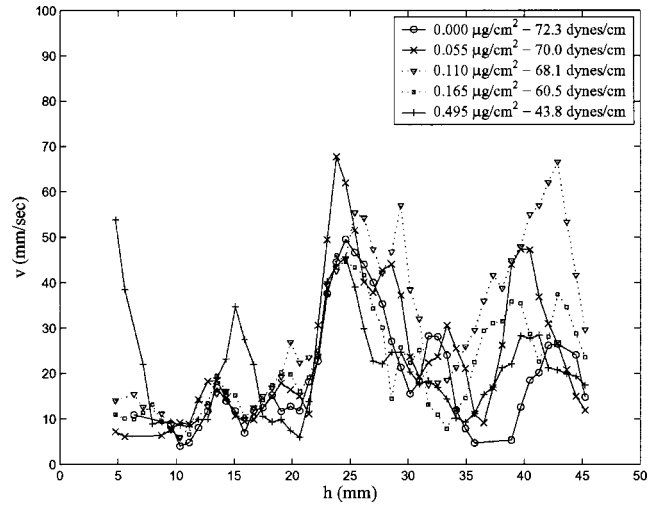


FIG. 9. Plot of v versus h for all experiment #1 concentrations tested. The water surface was covered with monolayers of oleyl alcohol having the concentrations indicated in the legend. The drop was free of surfactants.

corded at a depth of 14 mm beneath the water surface. The increments between successive drop heights are 1/32 inch (0.79 mm). Values of h for which no data is recorded correspond to heights where the measured velocity fell beneath the minimum acceptable threshold. To reduce the scatter in these plots, velocities were averaged over a sliding bin window comprised of three drop heights (a distance of 2.4 mm). This averaged form of the data is shown in Fig. 8. Unless otherwise noted, these averaged plots are what is presented in subsequent figures.

Figure 9 shows the experiment #1 v versus h data for all oleyl alcohol concentrations tested. Peaks are visible in these plots at drop heights of $h \approx 5, 15, 25,$ and 40 mm. The peaks near 25 and 40 mm are largest and will be used as a basis for comparison between the two experiments in subsequent discussions. These peaks will be referred to by their nominal drop height (e.g., peak 25 is the peak near a drop height of

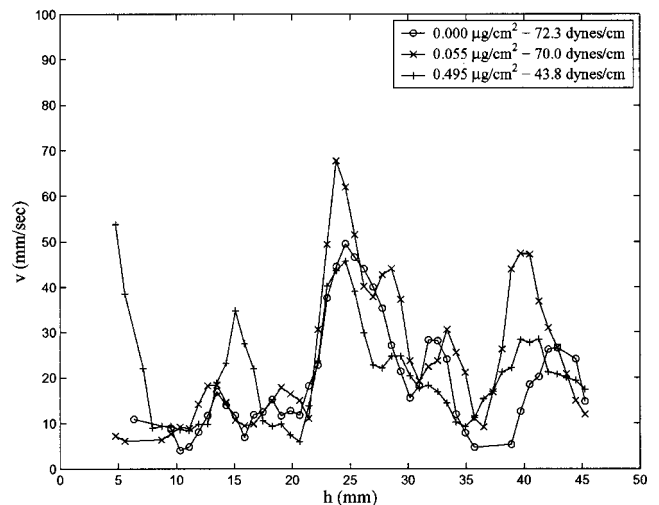


FIG. 10. Plot of v versus h for some experiment #1 data. Data for a surfactant free surface and data for two oleyl alcohol covered surfaces are shown.

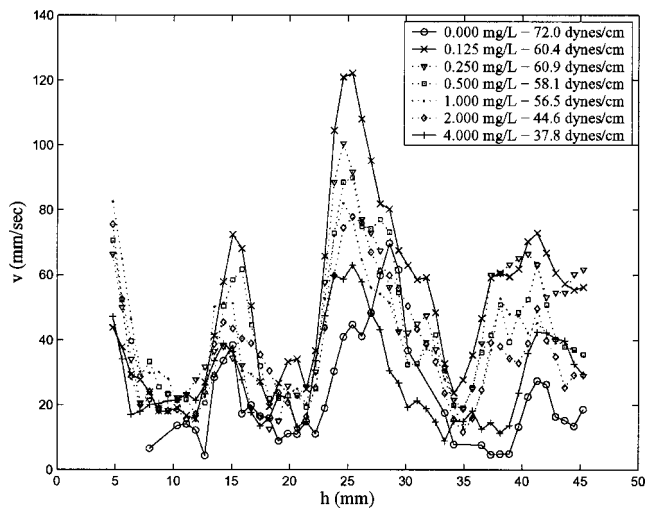


FIG. 11. Plot of v versus h for all experiment #2 runs. The Triton X-100 concentrations are indicated in the legend. The drops were free of surfactants.

25 mm) even though these locations may vary somewhat from concentration to concentration and also from experiment #1 to experiment #2. Some peaks are “jagged,” which is believed to be a remnant of the scatter, incompletely removed by the averaging procedure.

The trends in the data presented in Fig. 9 are difficult to discern because of the multiple data sets that are presented. To reveal better the effect of surfactant concentration, Fig. 10 includes only three concentrations. This figure shows that, for both peaks 25 and 40, the largest vortex velocity occurs at an intermediate surfactant concentration of $0.055 \mu\text{g}/\text{cm}^2$. The zero concentration condition ($c=0 \mu\text{g}/\text{cm}^2$) and the largest concentration case ($c=0.495 \mu\text{g}/\text{cm}^2$) both give a lower vortex velocity. This point will be elaborated upon.

The variation in v with concentration is less clear at lower drop heights. The reason for this is thought to be due to increased drop shape sensitivity. As discussed in the Introduction, it has been demonstrated that vortex penetration is a

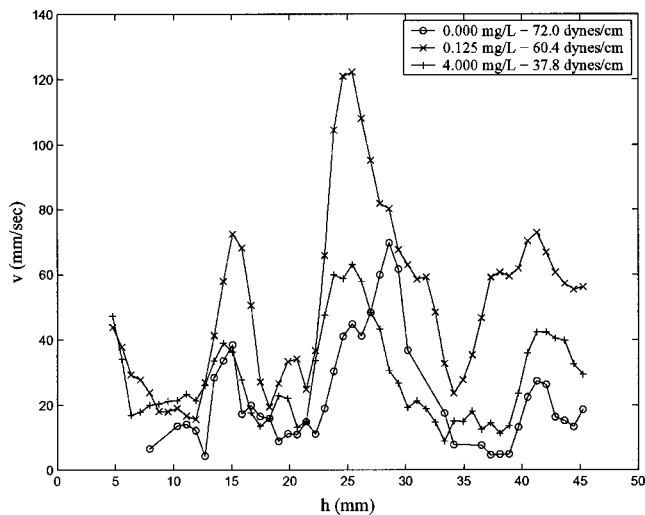


FIG. 12. Plot of v versus h for experiment #2 runs. Only some of the data from Fig. 11 are included to simplify the presentation.

TABLE II. Drop height ranges used to compute v_p for peaks 25 and 40.

	Peak 25	Peak 40
Experiment #1	23.5.0–27.5 mm	38.5–43.0 mm
Experiment #2	23.5.0–27.5 mm	38.5–43.0 mm

function of drop shape at the moment of impact.^{4,8,9} At locations near the nozzle, the drop oscillations occur close together in space, since the fall velocity is small at these locations. As a result, drop shape at the moment of impact is more sensitive to slight differences in the breakoff dynamics of the drop when the drop is released from a low height.

Figure 11 shows the v versus h data collected for experiment #2 where water drops impacted a surface having a Triton X-100 monolayer. All concentrations tested are included in this figure. The peak vortex velocity locations are very similar to those found in experiment #1. This is expected because the drop properties were not altered, and therefore the drop oscillation patterns during free fall should be the same, as should the drop shape at impact. The peaks in these plots are more pronounced than those seen in experiment #1.

Figure 12 presents only three of the concentrations presented in Fig. 11 to facilitate comparison. The effect of surfactant concentration on v is the same as for experiment #1. Maximum v occurs at an intermediate concentration of $c = 0.125 \text{ mg}/\text{L}$ for peaks 25 and 40. The zero concentration case and the highest concentration case ($4.0 \text{ mg}/\text{L}$) both resulted in a slower vortex velocity.

To reveal better the effect of surfactant concentration on vortex velocity, the data presented in Figs. 9 and 11 are distilled in the form of peak vortex velocity versus concentration plots. Peak vortex velocity v_p is the velocity at each of the two peaks (25 and 40). To eliminate sensitivity to the jagged nature of some of these peaks, data were averaged in a window around each peak. The windows used to obtain v_p are presented in Table II.

Plots of v_p versus c are presented in Figs. 13–16 for oleyl alcohol at peak 25, oleyl alcohol at peak 40, Triton

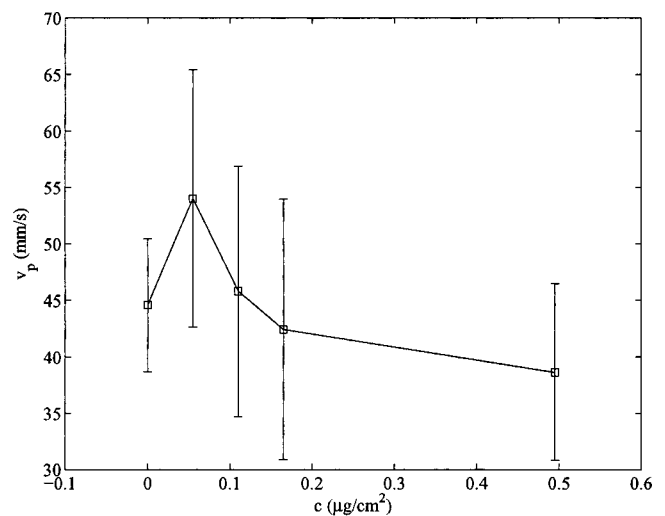
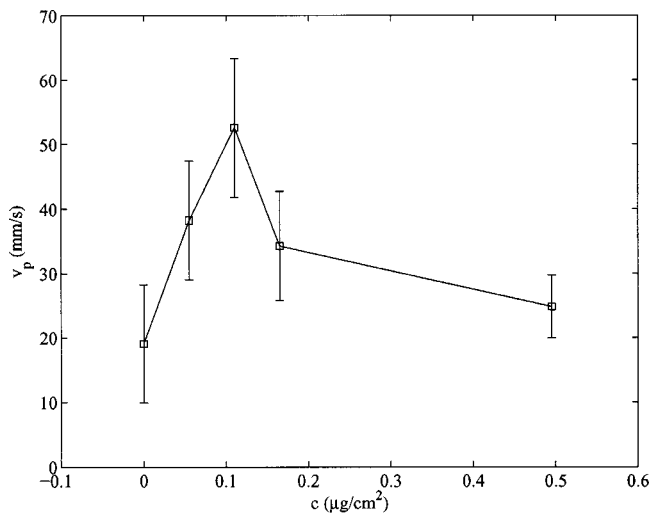
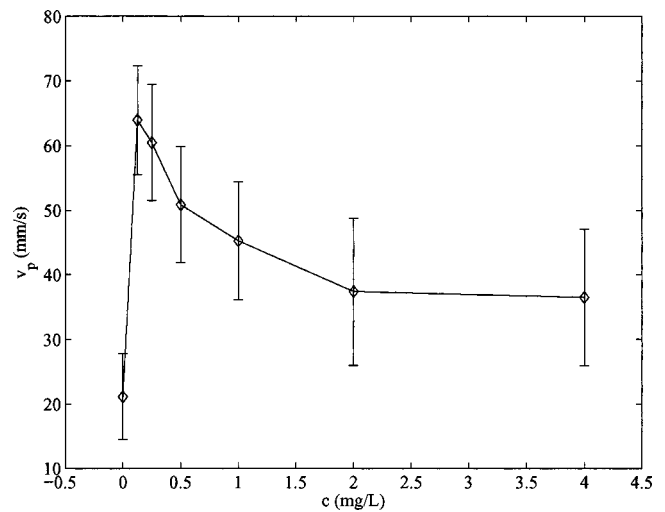


FIG. 13. Experiment #1 v_p versus c for peak 25.

FIG. 14. Experiment #1 v_p versus c for peak 40.FIG. 16. Experiment #2 v_p versus c for peak 40.

X-100 at peak 25, and Triton X-100 at peak 40, respectively. Included in each figure are 95% confidence intervals, obtained assuming a normal distribution of the data.¹⁷ For all but Fig. 13, the confidence interval at the intermediate surfactant concentration does not overlap that at either the highest or lowest concentration, permitting us to draw conclusions about the behavior at these three concentrations. For all four plots, the intermediate surfactant concentrations results in the highest vortex velocity.

It was observed that a given surfactant concentration did not always result in the same surface tension. Within a given run, or from run-to-run, variations in surface tension were observed for a given surfactant concentration. Possible reasons for this include surfactant loss, and errors in surfactant deposition. These errors were not large, however, a concern was that v_p versus σ plots would show behavior different than the v_p versus c plots. This turned out not to be the case; the peak in v_p versus σ plots was located at a surface tension corresponding to the surfactant concentration where a peak was located in the corresponding v_p versus c plots. An example of a v_p versus σ plot is presented in Fig. 17, which is

analogous to Fig. 14. Of course the plot is flipped since surface tension decreases with increasing surfactant concentration.

IV. DISCUSSION

The goal of these experiments was to determine if surfactant monolayers affect the penetration velocity of drop-induced vortex rings. The data presented in Figs. 13–16 indicate that they can. The large 95% confidence intervals in these figures restrict the conclusions that can be drawn to some extent. However, in Figs. 14–16 it can be stated with a confidence of 95% that the vortex velocities at the intermediate concentrations are larger than the vortex velocities at the maximum or minimum concentrations. It is only in Fig. 13 that the confidence intervals are too large to state this with confidence. A possible explanation for these observations is now presented.

The plots of peak vortex velocity versus surfactant concentration presented in Figs. 13–16 are reminiscent of the

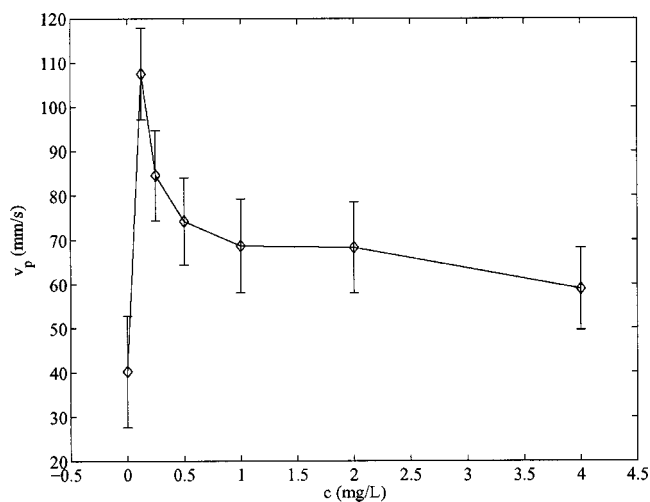
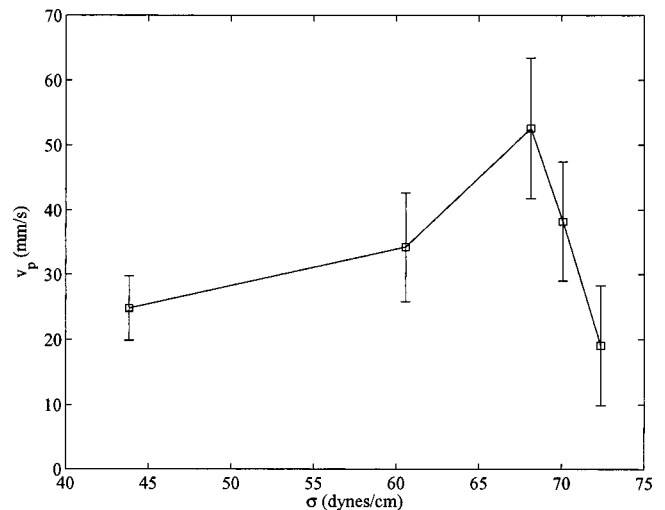
FIG. 15. Experiment #2 v_p versus c for peak 25.

FIG. 17. Plot of peak vortex velocity versus surface tension for oleyl alcohol monolayers (experiment #1), near the 40 mm peak.

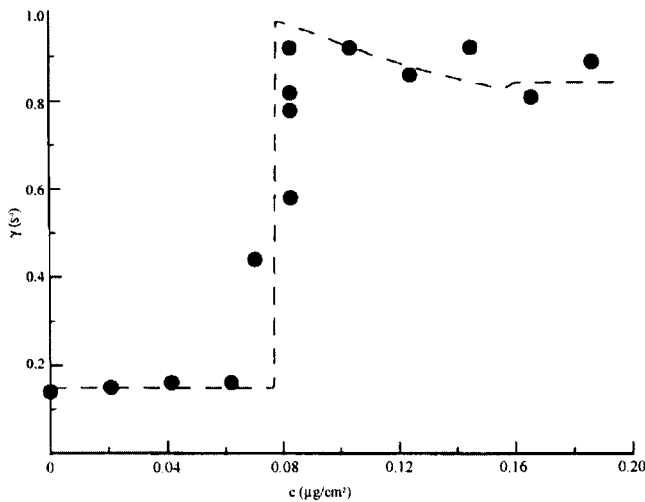


FIG. 18. Plot of capillary wave damping rate versus oleyl alcohol concentration. Figure due to Henderson (Ref. 21).

effect that surfactants have on capillary wave damping coefficients. A significant body of literature exists concerning surfactant damping of capillary waves. The general behavior that has been observed shows an initial increase in the damping coefficient as the surfactant concentration increases. The damping coefficient reaches a maximum and then decreases with further increase in concentration. This has been observed for a variety of surfactants. For example, Lucassen and Hansen¹⁸ observed this behavior for octanoic acid and lauryl amine hydrochloride, McGivern and Earnshaw¹⁹ for glycerol monooleate, and Noskov and Zubkova²⁰ for stearic acid and palmitic acid. Many other references exist.

Of particular interest here is the work of Henderson²¹ and Lapham *et al.*²² who show the behavior described above for oleyl alcohol and Triton X-100, respectively. The data of Henderson²¹ are presented in Fig. 18, showing a large increase in the wave damping coefficient for oleyl alcohol at $c \approx 0.08 \mu\text{g}/\text{cm}^2$ followed by a decrease beyond this peak value.²³ The v_p versus c data for oleyl alcohol at peak 40 is replotted in Fig. 19 to match Henderson's x axis. For the

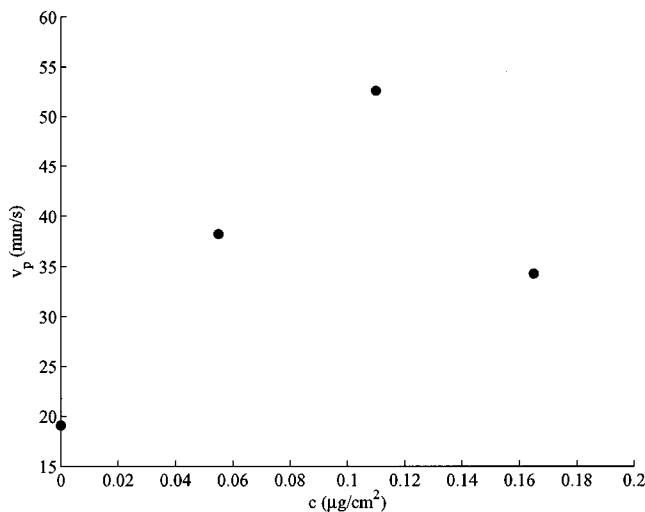


FIG. 19. Experiment #1, v_p versus c at peak 40.

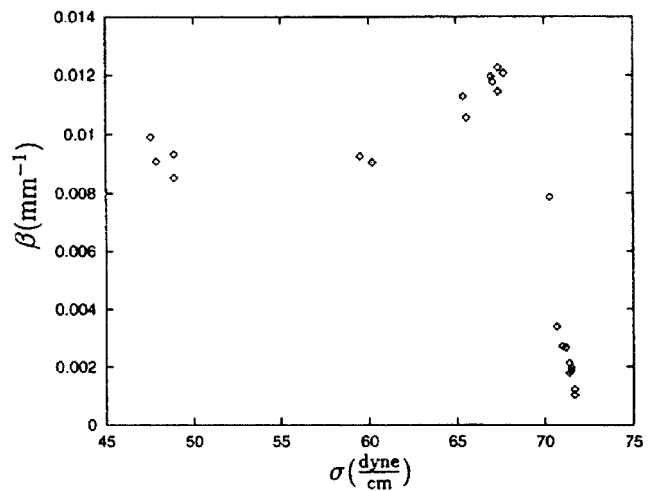


FIG. 20. Plot of β versus σ for Triton X-100. Figure obtained from Lapham *et al.* (Ref. 22).

Henderson plot and the vortex velocity data of the present work, a peak occurs at $c = 0.08$ and $0.1 \mu\text{g}/\text{cm}^2$, respectively, a difference of only $0.02 \mu\text{g}/\text{cm}^2$. The data in Fig. 19 are sparse. Greater resolution on the x axis might reveal a peak even closer to that of Henderson.

Lapham *et al.*²² showed the effects of Triton X-100 on the capillary wave damping coefficient. Figure 20 presents Lapham's damping coefficient data plotted against surface tension. Because surface tension decreases with increasing surfactant concentration, these β versus σ plots are analogous, but flipped versions of the plots due to Henderson. Lapham's plot shows a peak value for wave damping at intermediate σ (between zero concentration and high concentration of Triton X-100). This plot is remarkably similar to the present v_p versus σ plots presented in Fig. 21, where the peak 40 vortex velocity data for Triton X-100 is replotted against surface tension. This curve resembles the wave damping data presented by Lapham. The peak of Lapham's plot occurs near 68 dynes/cm while the peak observed in the v_p versus σ data obtained here occurs near 61 dynes/cm, a

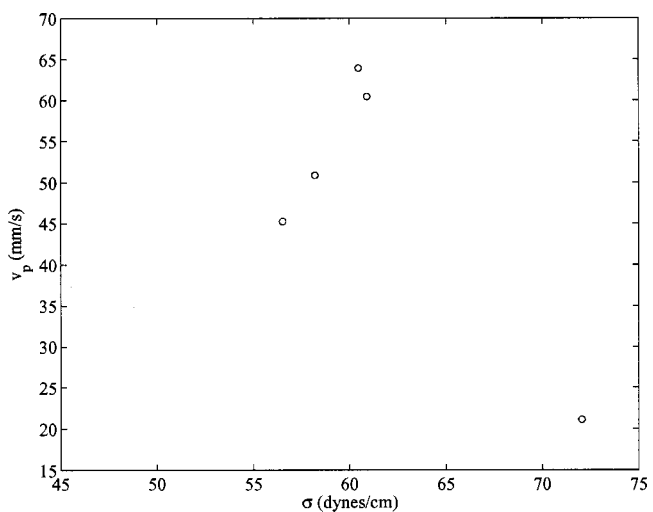


FIG. 21. Experiment #2 v_p versus surface tension σ for peak 40.

difference of only 10%. Vortex velocity data were not collected near 68 dynes/cm in the Triton X-100 experiments so the two peaks may coincide to an even greater degree.

The similarity in the peak location and shape of the v_p versus c plots presented here, and the wave damping coefficient versus c plots of Henderson²¹ and Lapham *et al.*²² suggests a possible relationship between capillary wave damping and vortex formation. Exactly what this relationship might be is unclear. Here we present a possible scenario.

Oguz and Prosperetti²⁴ analyzed the processes which occur when a drop impacts a water surface. Their analysis revealed that the process by which the drop and flat surface become one is dominated by the approach velocity of the drop and the flat surface. Moreover, they found that at the moment of impact, capillary waves begin to propagate along both the drop interface and the flat water interface. As the drop and flat surface continue to approach each other, the peaks of the capillary waves touch, enclosing thin toroids of air centered at the impact point. Although the authors did not move their analysis further forward in time, they speculate that these toroids will quickly become unstable and break up into very small bubbles. These results are supported by the work of Mesler and co-workers^{25,26} who observed very small bubbles entrained by drop-induced vortices.

The relevance of the work of Oguz and Prosperetti²⁴ to the present work is the presence of capillary waves. If drop impacts follow the course described by these authors, then the presence of surfactant monolayers at the flat surface should suppress the formation of capillary waves. This capillary wave suppression would in turn suppress the formation of air toroids and bubbles. We presume that suppression of bubble formation would be beneficial to vortex penetration; bubbles have buoyancy which would serve to obstruct any downward motion. If this is indeed the case, then the capillary wave suppression at the drop impact zone should occur in a fashion similar to that observed by Henderson²¹ or Lapham *et al.*²² described above. This would explain why the vortex velocity data presented here follow the same trend as the capillary wave damping data. We note that Esmailzadeh and Mesler²⁶ found that clean surfaces were important for the observation of Mesler entrainment, further supporting the above hypothesis. Also, Pumphrey and co-workers have observed that bubble entrainment by drops is affected by surfactants for bubble entrainment other than Mesler entrainment (e.g., single bubble entrainment).^{27,28}

The presence of bubbles was not observed in the present work. However, we were not looking for them when these experiments were conducted. Moreover, the experimental procedure employed by Mesler seems to indicate that these bubbles are difficult to observe. Indeed, Esmailzadeh and Mesler²⁶ purposely avoid adding dye to their drops out of a concern that the dye might obscure the small bubbles. Hence, such bubbles easily may have been present during our experiments.

Another explanation for the observations presented here concerns possible surfactant damping of waves that are caused, not by the drop impact, but due to environmental vibrations such as building vibrations. These waves would be damped out by surfactant monolayers also. If rough surface

conditions interfere with vortex formation, then vortex velocity would then be increased when surfactants are present in intermediate concentrations. This possibility is just as relevant to the limnological and oceanic applications described earlier since capillary waves are present during even the slightest of breezes on these water surfaces.

Further testing is necessary to confirm or refute the above ideas. At the present time, the most definitive statement that can be made is that the vortex penetration velocity of drop-induced vortices is affected by the presence of surfactants in a fashion that is very similar to how surfactants damp capillary waves. This was found to be true for both the insoluble surfactant, oleyl alcohol and the soluble surfactant, Triton X-100.

One of the fields where this research finds application is in rain-enhanced oxygenation of lakes. As was discussed in the Introduction, a peak in oxygen concentration was found by Durst⁸ at depths beneath the surface, a result which is explainable by rain induced vortices transporting surface oxygen below the surface. The present results show that such vortices would benefit from the presence of surfactants. Due to bioactivity, lakes have natural surfactant monolayers which can be expected to be present virtually all of the time. Therefore, it can be expected that these surfactants will enhance the transport of oxygen by vortices which are formed by raindrop impacts, a natural benefit for lakes. This would also be true for oceanic transport of carbon dioxide.

V. CONCLUSION

The effect of surfactant monolayers on the development of vortices formed by a drop impact was investigated. Surfactants were placed on the flat water surface, while the drop fluid was kept free of surfactants. Measurements of vortex velocity beneath the water surface indicated that surfactants actually increased the vortex velocity over that observed on a surfactant-free surface. Peak vortex velocities were observed for intermediate surfactant concentrations. Beyond this intermediate surfactant concentration, further increases in surfactant concentration resulted in a decrease in vortex velocity. These observations were true for both an insoluble surfactant (oleyl alcohol), and a soluble surfactant (Triton X-100). A possible mechanism based on the damping of capillary waves by surfactants is discussed, although this mechanism cannot be definitively supported by the results. These results have special significance for rain enhanced oxygenation of lakes where natural surfactants are omnipresent and therefore may serve to enhance limnological oxygenation during rain.

ACKNOWLEDGMENTS

This work was supported by Clemson University. The authors would like to thank Professor Donald E. Beasley for loaning several crucial pieces of instrumentation.

¹W. B. Rogers, "On the formation of rotating rings by air and liquids under certain conditions of discharge," *Am. J. Sci.* **26**, 246 (1858).

²J. J. Thomson and H. F. Newall, "On the formation of vortex rings by drops falling into liquids and some allied phenomena," *Proc. R. Soc. London* **39**, 417 (1885).

³The present work relates to changes in surface tension due to surfactant

- monolayers, and how these changes affect drop induced vortex formation. One of the conclusions of Thomson and Newall (Ref. 2) was that the absence of surface tension promotes the formation of vortex rings. Careful reading of their work reveals that their reference to surface tension does not refer to the surface tension between the liquid and the air, but rather the surface tension between the vortex ring fluid and the bulk fluid, which is zero when the drop fluid and bulk fluid are the same, as is the case in the present study.
- ⁴D. S. Chapman and P. R. Critchlow, "Formation of vortex rings from falling drops," *J. Fluid Mech.* **29**, 177 (1967).
- ⁵We note in passing that drops falling at velocities approaching terminal velocity will oscillate about a nonspherical drop shape (Refs. 6 and 7). The velocities for drops falling from the low drop heights considered here are much less than terminal velocity and should, therefore, oscillate about an approximately spherical shape.
- ⁶K. V. Beard and C. Chuang, "A new model for the equilibrium shape of raindrops," *J. Atmos. Sci.* **44**, 1509 (1987).
- ⁷K. V. Beard, H. T. Ochs, and R. J. Kubesh, "Natural oscillations of small raindrops," *Nature (London)* **342**, 408 (1989).
- ⁸F. Durst, "Penetration length and diameter development of vortex rings generated by impacting water drops," *Exp. Fluids* **21**, 110 (1996).
- ⁹F. Rodriguez and R. Mesler, "The penetration of drop-formed vortex rings into pools of liquid," *J. Colloid Interface Sci.* **121**, 121 (1988).
- ¹⁰B. Peck, L. Sigurdson, B. Faulkner, and I. Buttar, "An apparatus to study drop-formed vortex rings," *Meas. Sci. Technol.* **6**, 1538 (1995).
- ¹¹D. T. Ho, L. F. Bliven, R. Wanninkhof, and P. Schlosser, "The effect of rain on air-water gas exchange," *Tellus, Ser. B* **49**, 149 (1997).
- ¹²D. T. Ho, W. E. Asher, L. F. Bliven, P. Schlosser, and E. L. Gordan, "On mechanisms of rain-induced air-water gas exchange," *J. Geophys. Res., [Oceans]* **105**, 24045 (2000).
- ¹³P. A. Lange, G. v. d. Graaf, and M. Gade, "Rain-induced subsurface turbulence measured using image processing methods," in *Proceedings of the 2000 International Geoscience and Remote Sensing Symposium (IGARSS 2000)* (IEEE, Piscataway, NJ, 2000), Vol. VII, pp. 3175-3177.
- ¹⁴R. C. Weast, *Handbook of Chemistry and Physics*, 52nd edition (CRC, Cleveland, OH, 1972).
- ¹⁵B. Peck and L. Sigurdson, "The three-dimensional vortex structure of an impacting water drop," *Phys. Fluids* **6**, 564 (1994).
- ¹⁶B. Peck and L. Sigurdson, "The vortex ring velocity resulting from an impacting water drop," *Exp. Fluids* **18**, 351 (1995).
- ¹⁷H. J. Larson, *Introduction to Probability Theory and Statistical Inference* (Wiley, New York, 1982).
- ¹⁸J. Lucassen and R. S. Hansen, "Damping of waves on monolayer-covered surfaces I. Systems with negligible surface dilational viscosity," *J. Colloid Interface Sci.* **22**, 32 (1966).
- ¹⁹R. C. McGivern and J. C. Earnshaw, "Observation of unusual effects in the damping of capillary waves on monolayer-covered surfaces," *Langmuir* **5**, 545 (1989).
- ²⁰B. A. Noskov and T. U. Zubkova, "Dilational surface properties of insoluble monolayers," *J. Colloid Interface Sci.* **170**, 1 (1995).
- ²¹D. M. Henderson, "Effects of surfactants on Faraday-wave dynamics," *J. Fluid Mech.* **365**, 89 (1998).
- ²²G. S. Lapham, D. R. Dowling, and W. W. Schultz, "Linear and nonlinear gravity-capillary water waves with a soluble surfactant," *Exp. Fluids* **30**, 448 (2001).
- ²³Note that the x axis in this figure differs by a factor of 100 from that presented in Henderson due to an error in Fig. 3(d) of Ref. 21 (personal communication with the author).
- ²⁴H. N. Oğuz and A. Prosperetti, "Surface-tension effects in the contact of liquid surfaces," *J. Fluid Mech.* **203**, 149 (1989).
- ²⁵K. Carroll and R. Mesler, "Part II: Bubble entrainment by drop-formed vortex rings," *AIChE J.* **27**, 853 (1981).
- ²⁶L. Esmailizadeh and R. Mesler, "Bubble entrainment with drops," *J. Colloid Interface Sci.* **110**, 561 (1986).
- ²⁷H. C. Pumphrey and L. A. Crum, "Underwater sound produced by individual drop impacts and rainfall," *J. Acoust. Soc. Am.* **85**, 1518 (1989).
- ²⁸H. C. Pumphrey and P. A. Elmore, "The entrainment of bubbles by drop impacts," *J. Fluid Mech.* **220**, 539 (1990).